Characterization and Modeling of UHF RFID Channels for Ranging and Localization

Daniel Arnitz, *Student Member, IEEE,* Ulrich Muehlmann, *Member, IEEE*, and Klaus Witrisal, *Member, IEEE*

***Abstract*—A comprehensive characterization and model of the UHF RFID channel is presented for narrowband through ultra-wideband tag localization systems. The analyses are based on ultra-wideband channel measurements in a warehouse portal, centered around 900 MHz. Measured scenarios include an electromagnetically transparent pallet and a pallet containing liquids, each for a portal shielded by metal backplanes and for a portal shielded by absorbing material. The presented analyses cover the individual channels to and from the tag, the feedback channel, and the backscatter channel, for bi- and monostatic reader setups.**

We find that the direct path is rarely dominant on the backscatter link despite clear line-of-sight conditions and directive reader antennas. The power ratio between the direct and all indirect paths ranges from -20 through 5 dB for the more common metal portal, and RMS delay spreads are in the range of $10-80$ ns. Since only the direct (line-of-sight) path carries the correct distance/direction information, tag localization in such portals requires high robustness with respect to weak line-of-sight components.

We also show that classical channel models in UHF RFID, despite predicting the incident power level at the tag accurately, produce far too optimistic estimates of channel parameters relevant to ranging and localization.

***Index Terms*—ultra-high-frequency radio-frequency identification (UHF RFID), channel characterization, ranging, positioning, localization, narrowband, wideband, ultra-wideband**

I. Introduction

Localization in UHF RFID has seen a lot of research in the past years, but no conclusive breakthrough [1]. Implemented ranging systems are mostly narrowband due to limitations enforced by tag design and regulations and thus share a common property: they cannot distinguish individual multipath components (MPCs), i.e., the range estimate is based on an "average path". This generally results in biased estimates and high standard deviations if the direct path is not the dominant MPC. As opposed to ultra-wideband (UWB) localization [2], the ranging error for narrowband systems depends on the shape of the entire channel impulse response (CIR), and in particular on the power ratio between the direct and indirect paths. Unfortunately there is little information available regarding the CIR of UHF RFID channels because wideband parameters are usually not investigated in the context of the narrowband RFID system.

This paper presents comprehensive analyses of the UHF RFID channel in a warehouse portal, including an evaluation of different models for this channel. The analyses are mostly based on single-channel measurements in order to keep them comparable to the literature, e.g., [3]–[5], and to keep them applicable to non-backscatter systems such as UHF/UWB hybrids, e.g., [6], [7]. A method to convert the results to backscatter channels can be found in [8], and is briefly discussed in Section VII.

The paper is organized as follows: A summary of wideband channel parameters and their influence on narrowband ranging is given in Section II. Sections III and IV discuss measurement and simulation (modeling) setup, respectively. Detailed channel analyses are presented in Section V for the empty portal and in Section VI for the portal with a pallet containing liquids passing through. The backscatter property of the channel and performance results of narrowband through ultra-wideband ranging methods are briefly discussed in Sections VII and VIII, respectively.

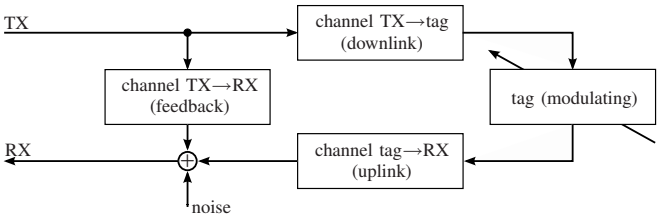

Fig. 1. Channels from the viewpoint of a passive RFID system. All channels are time-variant and may only be assumed to be short-time-stationary.

II. Channel Parameters and their Influence on Ranging and Localization Accuracy

From the viewpoint of backscatter-based localization, the channels are structured as shown in Fig. 1. The backscatter channel is formed by the concatenation of downlink channel (TX→tag), the tag's reflection coefficient, and the uplink channel (tag→RX). This combined channel is the basis for all backscatter-based localization methods; individual channels are not accessible. The feedback (TX→RX) incorporates all parts of the received signal that have not been modulated by the tag, i.e., mismatches at the antenna port for monostatic[1] setups, direct coupling for bistatic setups, as well as unmodulated environmental reflections (clutter). For the presented analyses, we will neglect the tag and focus on the wireless channels.

We define the power-delay-profile (PDP) as the squared magnitude of the CIR, and the average power-delay-profile (APDP) as a spatial average of PDPs. The first arriving component of CIR and (A)PDP corresponds to the line-of-sight (LOS) path between transmitter and receiver and

D. Arnitz and K. Witrisal are with the Signal Processing and Speech Communication Laboratory, Graz University of Technology, Graz, Austria (e-mail: daniel.arnitz@tugraz.at, witrisal@tugraz.at).

U. Muehlmann is with NXP Semiconductors, Gratkorn, Austria (e-mail: ulrich.muehlmann@nxp.com).

This work has been funded by NXP Semiconductors Austria and by the Austrian Research Promotion Agency (FFG) under the grant number 818072.

[1] monostatic: TX=RX-antenna, bistatic: separate TX and RX antennas

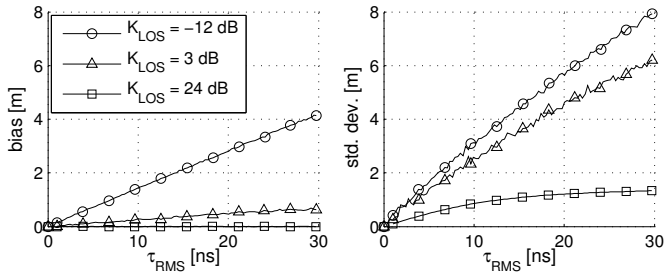

Fig. 2. Influence of wideband channel parameters (K_{LOS} and τ_{RMS}) on narrowband ranging accuracy (TX→tag only, 10^5 samples per parameter combination). The plots show bias and standard deviation for a phase-based ranging method [12] with 1 MHz bandwidth. Channels are simulated and follow an exponential APDP [13].

all following components correspond to indirect (reflected) paths. The square root of the second central moment of the normalized (A)PDP is called RMS delay spread (τ_{RMS}), while the last significant delay is referred to as the maximum excess delay, cf. [9]. For localization the power ratio of the direct (LOS) path to all indirect paths is of vital importance, as it quantifies the influence of the direct path on the entire delay-profile. Due to its similarity with the Ricean K-factor [10] we denote this ratio "line-of-sight K-factor" (short: K-factor), K_{LOS}. Note that K_{LOS} and the Ricean K-factor may be identical in some cases, but are not so in general.

The CIR, and thus parameters like K_{LOS} and τ_{RMS}, is only visible to systems with (ultra-)wide bandwidths due to the fine temporal resolution required to resolve MPCs. For narrowband systems the channel is represented by a single complex gain factor with random attenuation and phase shift, and some random group delay. Nonetheless, the shape of the underlying CIR has a massive influence on these parameters and hence on the performance of narrowband ranging. For high K-factors, the direct path is dominant in the group delay of a narrowband signal and narrowband ranging will give accurate results, cf. Fig. 2. For low K_{LOS}, on the other hand, the group delay is mainly determined by indirect paths. Depending on the RMS delay spread and the shape of the CIR, this results in a bias towards indirect (i.e., longer) paths and a high standard deviation of narrowband range estimates. See [11, pp. 44–47] for a more detailed discussion.

Depending on the employed localization method, also correlation in space and frequency has a strong influence on accuracy. These correlations are described by coherence distance and coherence bandwidth respectively, cf. [9], [10], [14]. The coherence distance is the spacing between two receivers at which the correlation between both CIRs drops below a given value (typ. 50, 70, or 90 %). It is important for array-based methods and for all approaches that combine estimates at two closely-spaced positions, e.g. [15]. In a similar fashion the coherence bandwidth specifies the frequency offset at which the autocorrelation of the channel transfer function (CTF) drops below a specified value. It is important for all methods that work in the frequency domain, for example by evaluating the phase shift between carriers [12], [16], [17].

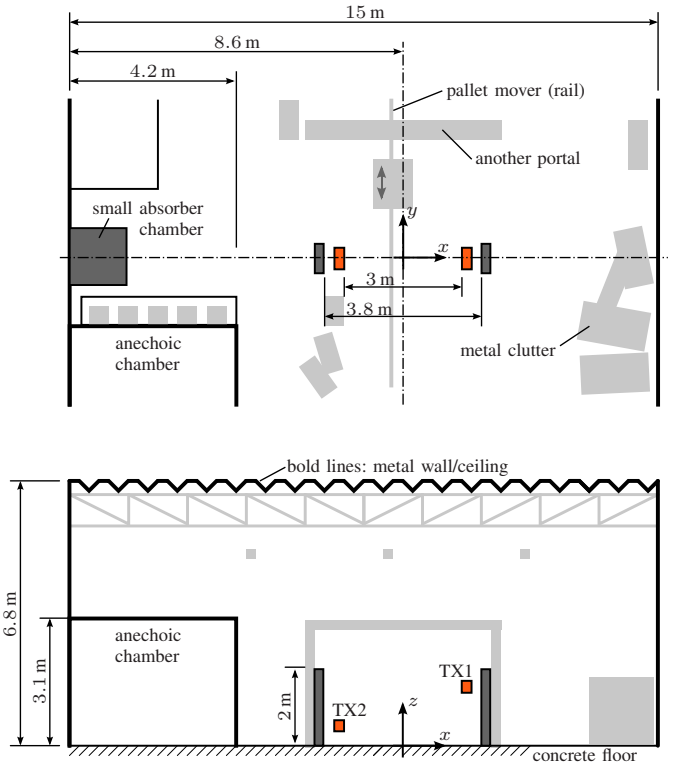

Fig. 3. Environment and portal setup (roughly to scale).

III. Measurement Setup

A. Environment Description

All measurements were performed in NXP's Application and System Center (ASC) in Gratkorn, Austria, in order to ensure a realistic warehouse environment. The ASC is located in a converted production hall (approx. $40 \times 15 \times 7$ m) with corrugated metal walls and ceiling, and a steel-reinforced concrete floor. The entire hall is cluttered with metal objects of different sizes (from boxes with screws to a room-sized anechoic chamber). A sketch of the measurement setup and its environment is shown in Fig. 3.

B. Gate Setup

The measurement setup (see Figs. 3 and 4) was constructed similar to a UHF RFID portal: The transmitter arrays were positioned 3 m apart (front to front) to the left and right of a pallet mover. The antenna heights were 0.5 m (TX2) and 1.5 m (TX1) respectively. The backplanes behind the transmitter antennas (80×195 cm, 22 cm from the back of the transmitter arrays) spanned a portal of 3.8 m width. Measurements were done with metal backplanes (typ. for portals, cf. [18]) and with absorber backplanes (reflectivity approx. -20 dB).

Receiver antennas were fixed at different x- and z-positions on polyurethane foam slabs, which were themselves mounted on the pallet, cf. Fig. 4. The pallet was then incrementally moved through the gate (along y) while recording. This was done for several positions on the pallet, thus forming planes of receiver positions with a grid spacing of 10 cm. All antennas were vertically polarized.

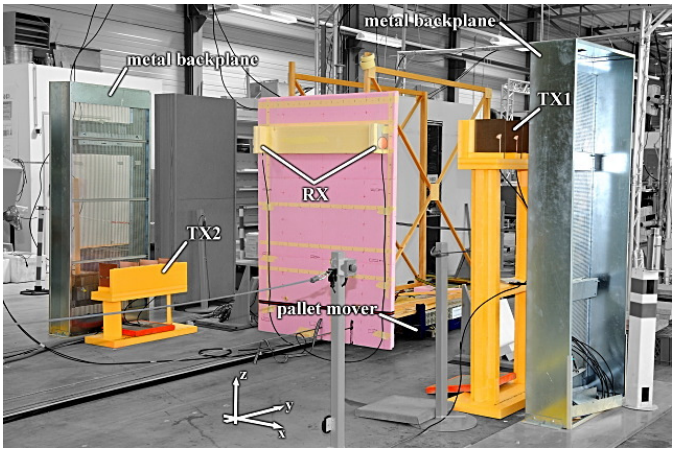

Fig. 4. Photograph of the gate setup with electromagnetically transparent pallet and metal backplanes (cf. [19, Fig. 3] and [20, Fig. 7]). The transmitter arrays are positioned on the orange stands. The receiver antennas are mounted on the pallet (pink polyurethane foam slab), moving through the portal.

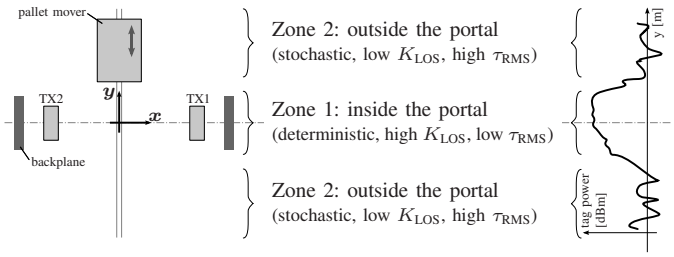

Fig. 5. Different channel properties for zones inside/outside the portal. Zone 3 covers the area far from the portal (stochastic, very low K_{LOS}, high τ_{RMS}).

The channel measurements were performed by a VNA in a frequency range of 0.5 through 1.5 GHz with 1 MHz stepsize. The conducted transmit power was 0 dBm and the resolution bandwidth was set to 10 kHz. The resulting ambiguity range is roughly 1 µs (maximum path length 300 m), and the resulting effective dynamic range is in the order of 100 dB[2]. The system was calibrated up to the antenna ports. Calibration of the remaining gain and delay was done using the known LOS distance and power. A more detailed description of the measurement setup, including full UWB directivity patterns of the used antennas, can be found in [20].

C. Pallet Description

Measurements were conducted with two different pallets. An electromagnetically transparent pallet (Fig. 4) constructed of a wooden scaffold and polyurethane foam slabs was used to measure the channels inside the empty portal. These measurements were done in four planes, two horizontal and two vertical ones, with 1364 receiver positions in total. The second pallet, containing liquids and metal-coated packages, acts as a challenging example for tag localization. Receiver antennas were mounted at the side of the liquids pallet, forming a single 2-dimensional plane with a partially blocked LOS to TX1 (620 positions in total). Further photographs and drawings are shown in [20].

[2]The dynamic range was limited by a high noise floor created by several active RFID readers and mobile phones in the immediate vicinity of the setup.

TABLE I
REFRACTIVE INDEX AND REFLECTION COEFFICIENT OF SURFACES.

Refractive Index	Value	Description
floor	2.5	concrete
gate	7	metal mesh w. antennas/cables in front
Reflection Coeff.	**Value**	**Description**
floor	0.5	concrete
gate	0.7	metal mesh w. antennas/cables in front
ceiling	0.8	metal, triangular structure (scatters)
wall (near floor)	0.35	obstructed by clutter (cf. Fig. 3)
wall (near ceiling)	0.8	unobstructed (cf. Fig. 3)

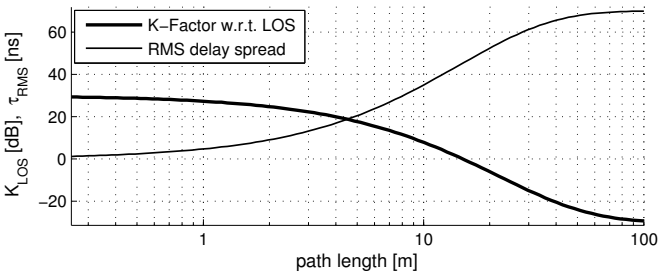

Fig. 6. Distance-dependent small-scale model parameters. See [11, Chapter 3] for a description and detailed explanation of these parameters.

D. Performed Analyses

The analyses presented in this paper are based on evaluations of APDPs as well as channel parameters extracted from instantaneous CTFs and PDPs. We use cumulative distribution functions (CDFs) and spatial ("3D") plots of instantaneous parameters to complement the "average channel" shown by the APDPs. Relevant reflections and clusters were identified manually using videos of the wave propagation derived from the measured CIRs[3].

Since UHF RFID utilizes directive antennas and often metal portals, it can be expected that "the typical UHF RFID channel" shows different behavior inside and outside the portal. Consequently, the environment was separated into three zones for the discussions, as shown in Fig. 5. Within the portal (zone 1, $|y| \leq 0.5$ m) the channel is dominated by the portal's geometry and thus highly deterministic, in particular for metal backplanes. In the vicinity of the portal (zone 2, $|y| \geq 1.0$ m) the gate's influence is smaller but still present. Zone 3, which is not covered by the presented measurements, spans the remaining space outside the vicinity of the portal and can most likely be modeled in a purely stochastic fashion (industrial non-line-of-sight). The transient zone between the inside of the portal and its vicinity, $0.5 \geq |y| \geq 1.0$ m, has been left out in order to avoid combining zones with different characteristics. A description of the individual estimators and calculations yielding the presented channel parameters was published in [20].

IV. Modeling and Simulation Setup

In addition to the analyses of the UHF RFID channel, this paper contains a comparison and validation of different models

[3]The propagation videos are available online along with other examples: http://www.spsc.tugraz.at/tools/paris-osf/examples

for this channel (Section V-C). The modeling was done using the PARIS simulation framework [11], a simulator designed for research on passive UHF RFID tag localization[4].

Depending on the simulated model (deterministic, stochastic, hybrid; see Section V-C), the simulations account for antenna directivity patterns (taken from measurements, cf. [20]), deterministic reflections created by portal and environment (gate backplanes, walls, ceiling, and floor), and stochastic scattering in the vicinity of the portal. A detailed description of the PARIS framework and its models can be found in [11, Chapter 3]. The model parameters used in this paper are listed in Table I and Fig. 6. These parameters were found manually using rule-of-thumb values (cf. [11, pp. 66f]) and by comparing the APDPs of measurement and simulation.

V. In-Depth Analyses: Empty Portal

The empty portal represents a baseline and best-case scenario for localization methods, with an unobstructed direct path and with little field distortions. Moreover, the results for the empty portal with absorber backplanes can also be taken as reference for applications in light multipath environments were only the floor acts as a reflector in the immediate vicinity.

We will start this in-depth analysis with a discussion of the APDP and the identification of major reflectors and clusters, followed by an analysis of the channel w.r.t. ranging and localization. Finally, we will discuss different models for this channel, including established UHF RFID channel models.

A. Discussion of the APDP / Source of Reflections

The APDPs for the empty portal with metal backplanes are shown in Fig. 7. Unsurprisingly, the backplanes are the dominant source of specular reflections. Up to five bounces can be identified, including multiple reflections between backplanes and the floor. Reflection at the walls close to the floor are blocked by the gate and scattered by clutter, thus making wall reflections relatively insignificant, cf. Fig. 3. This is, on the other hand, not true for a double reflection via the ceiling close to the walls, which is not obstructed by the backplanes for either transmitter. Unlike the floor, the ceiling is free of clutter, thus allowing the wave to bounce between the outer walls of the hall several times. The APDP shows at least nine reflections of this specific wave packet, six of which are within $100\,\mathrm{m}$ and thus visible in Fig. 7.

Note that the general shape of the APDP inside the gate follows a power law [22] instead of the commonly assumed exponential decay. Also the clusters created by the wall-reflections close to the ceiling follow a power law in their decay. This behavior, which is consistent with a mainly deterministic channel, cf. [23], is highlighted in Fig. 8. A similar behavior of the ray power decay in industrial environments has been reported previously in [22]. Outside the portal, most of the APDP follows an exponential decay.

B. Discussion of Wideband Channel Parameters

Key channel parameters for ranging and localization are LOS K-factor, RMS delay spread, coherence bandwidth

[4]The framework is open-source and available online [21].

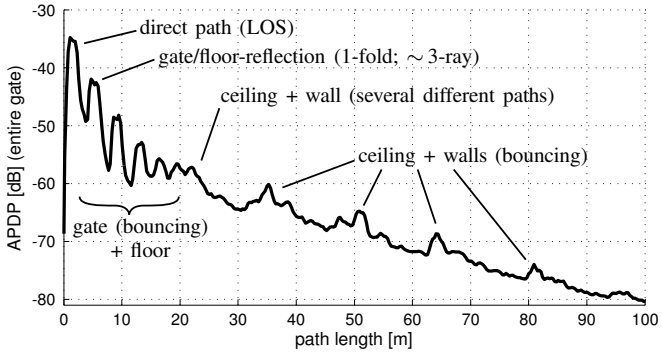

Fig. 7. Average power-delay-profile (APDP) for TX1 with marked clusters (empty gate, metal backplanes).

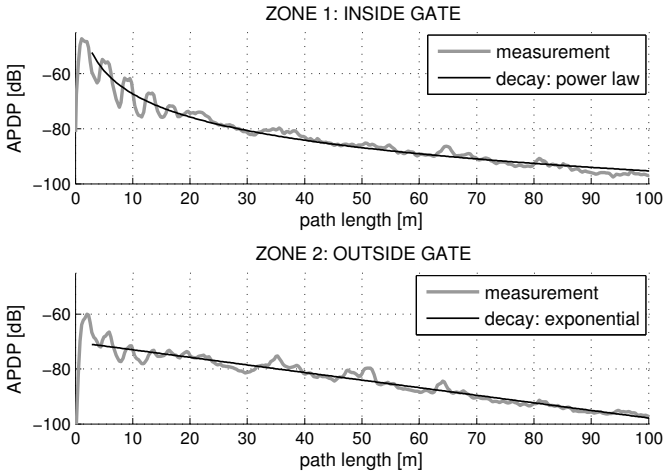

Fig. 8. Average power-delay-profile for TX1 inside and outside the portal (empty portal, metal backplanes). The APDP inside the gate follows a power law instead of the commonly assumed exponential decay.

(which is loosely coupled to the RMS delay spread [9], [14]), and the coherence distance. Although LOS K-factor and RMS delay spread in particular are wideband parameters, they play a central role also for narrowband (and to some extent ultra-wideband) localization, as discussed in Section II.

Spatial distributions of K_{LOS} and τ_{RMS} are shown in Fig. 9 for metal and absorber backplanes. The influence of the backplanes on K_{LOS} and τ_{RMS} is quite pronounced: The K-factor drops by $8\,\mathrm{dB}$ inside and $3\,\mathrm{dB}$ outside the portal for metal backplanes compared to absorbing material. At the same time the RMS delay spread increases by $40\,\%$ inside the portal and by $5{-}10\,\%$ in its vicinity.

CDFs of both parameters can be found in Fig. 10(a)-(b). The K-factor for the more common metal backplanes is in the range of -6 through $2\,\mathrm{dB}$ outside and -1 through $6\,\mathrm{dB}$ inside the gate. The RMS delay spread for the metal portal ranges from roughly $10{-}25\,\mathrm{ns}$ inside the gate to $40{-}55\,\mathrm{ns}$ outside. CDFs of the last two channel parameters, $90\,\%$ coherence distance and $90\,\%$ coherence bandwidth, are displayed in Fig. 10(c)-(d). The $90\,\%$ coherence distance is always below $10\,\mathrm{cm}$, (i.e., a third of the wavelength at $900\,\mathrm{MHz}$) outside the portal, but reaches almost twice the wavelength ($50\,\mathrm{cm}$) inside the gate. Note that the portal width limits the observable coherence

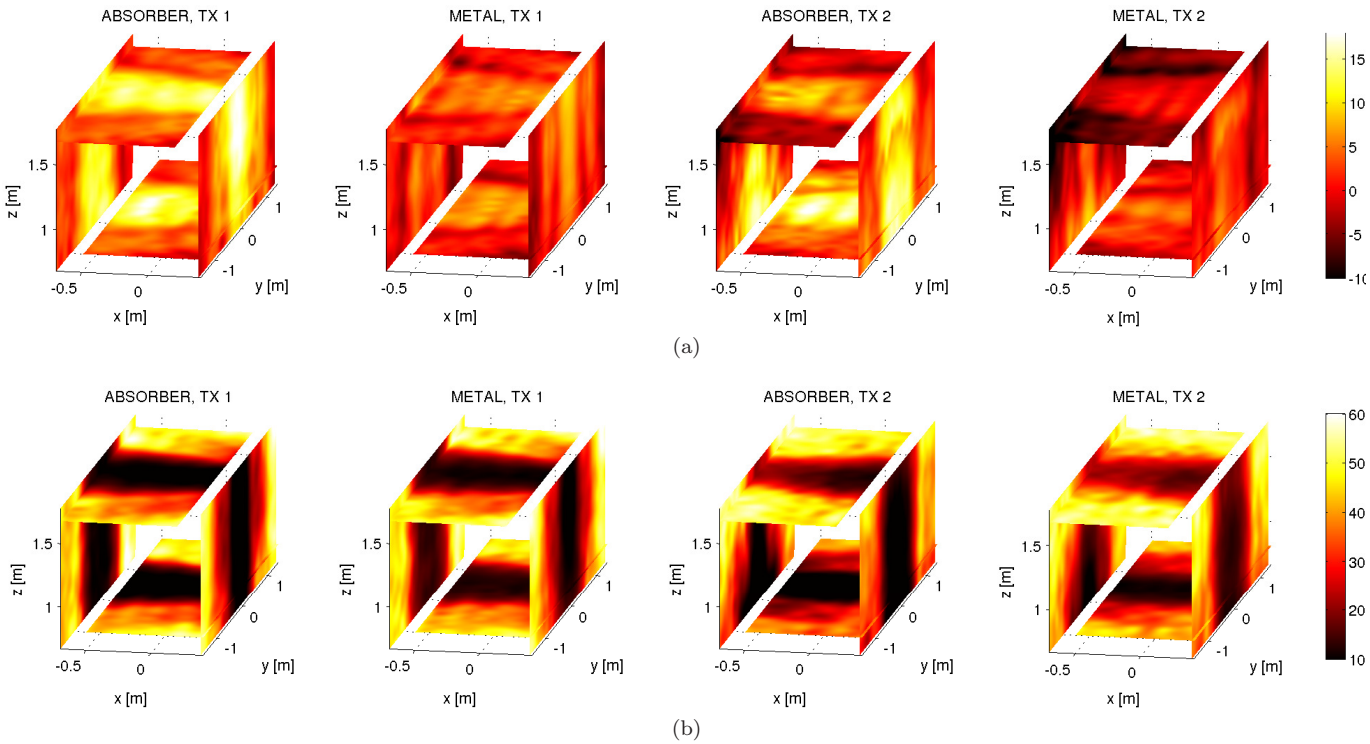

Fig. 9. (a) K-factor [dB] and (b) RMS delay spread [ns] for the empty portal, comparing metal and absorber backplanes (cf. [20, Fig. 19]).

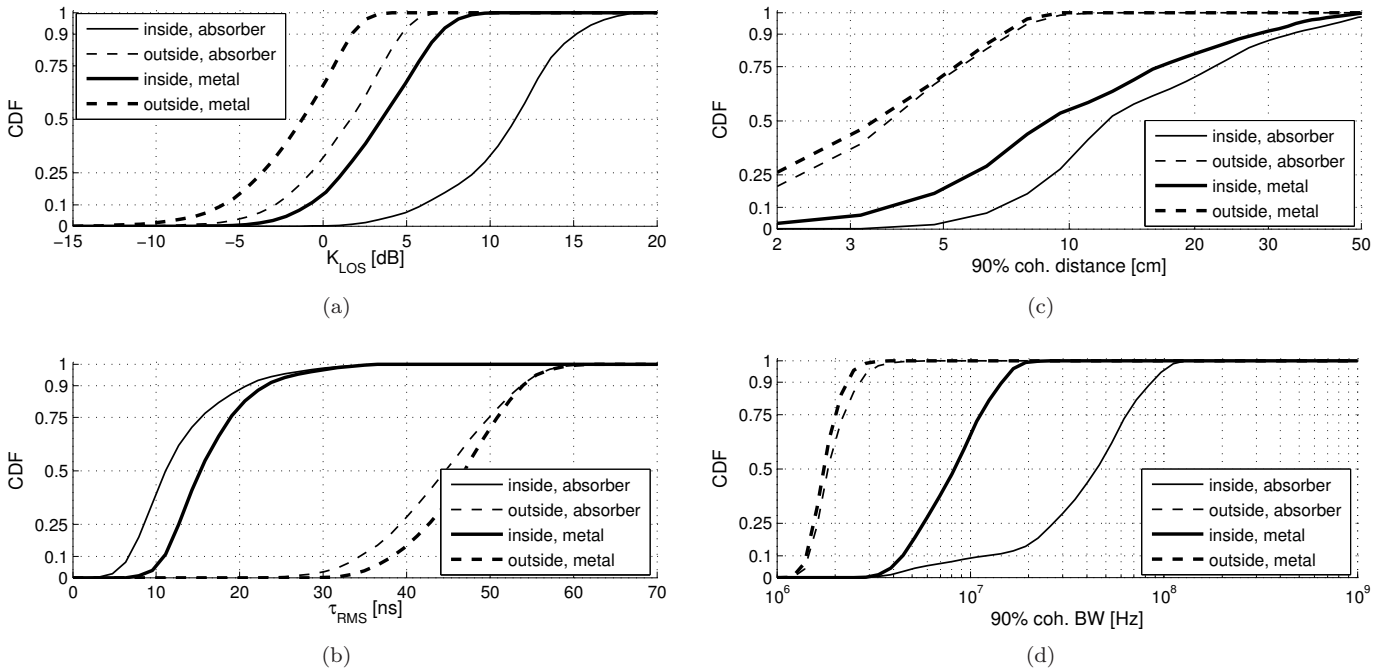

Fig. 10. CDFs for the empty portal. (a) K-factor, (b) RMS delay spread, (c) 90 % coherence distance, (d) 90 % coherence bandwidth. Note that the gate geometry limits the observable coherence distance to roughly 40 cm.

distance to roughly 30−40 cm, cf. [20], hence the correlation inside the portal is likely underestimated. The coherence bandwidth ranges between 1 and 3 MHz outside the portal. It reaches 20 MHz inside the portal for metal backplanes and 100 MHz for absorbing material. However, it may be as low as 3 MHz also inside the portal.

C. Validation of Common Channel Models

In this section, we will discuss the validity of three basic types of channel models:

1) A purely stochastic channel model with random CIRs (only the LOS is deterministic) derived from an exponential APDP [13]. The purely stochastic model thus

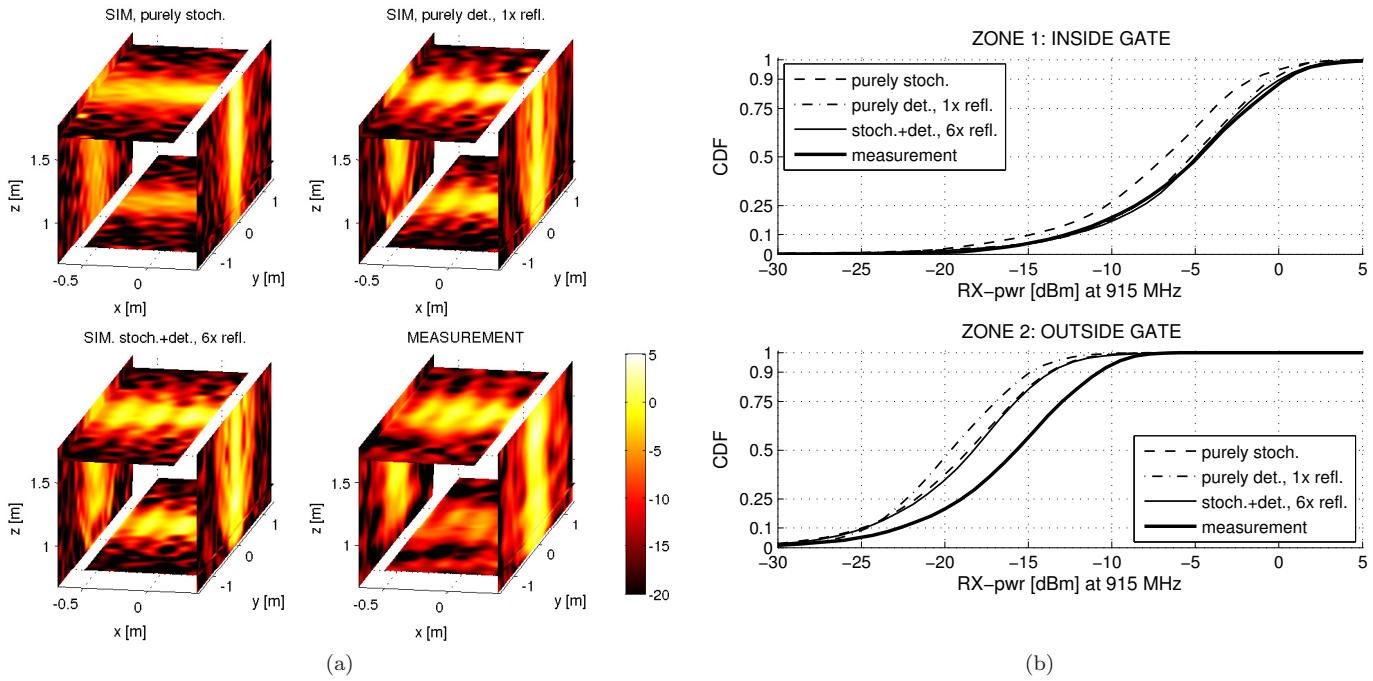

Fig. 11. Incident power level [dBm] at the tag for the empty portal with metal backplanes (carrier frequency 915 MHz, transmit power 3.28 W EIRP). Comparison between models of different complexity and measurement: (a) spatial distribution with TX1 being active, (b) CDFs.

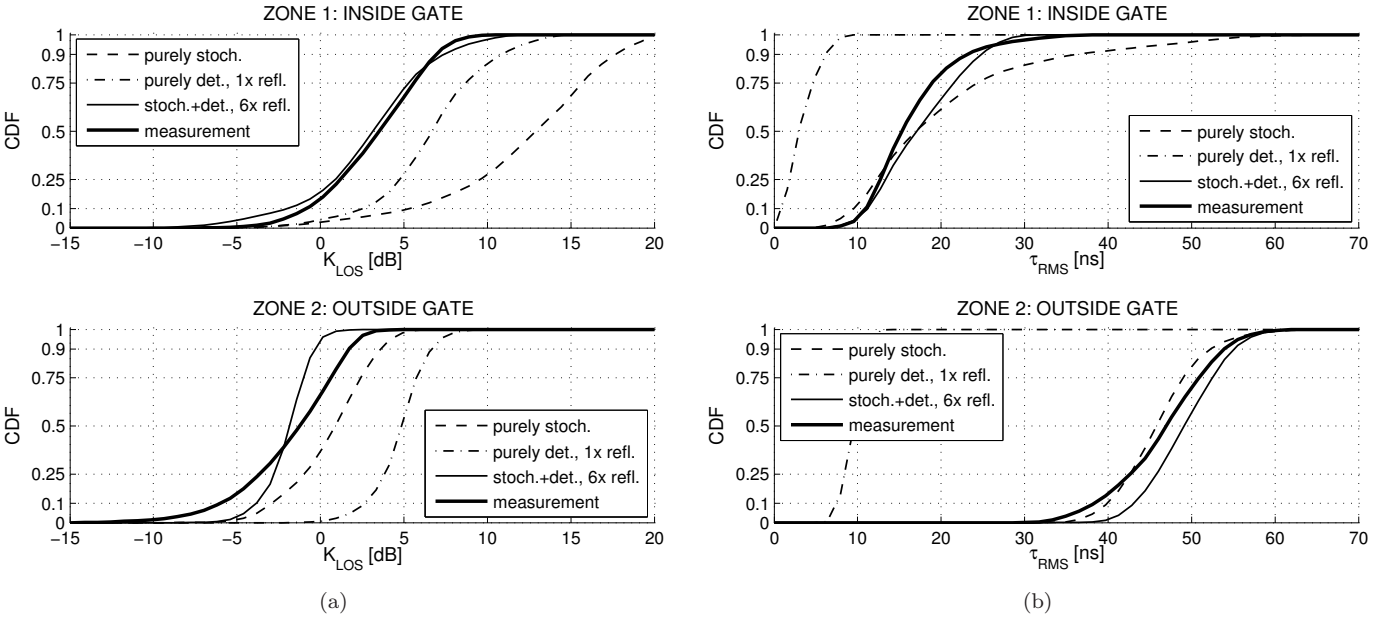

Fig. 12. Comparison between models of different complexity and measurement for the empty portal with metal backplanes: CDFs of (a) K-factor and (b) RMS delay spread.

considers scattering, but neglects specular reflections. It represents the statistical models commonly used for UWB channels, e.g., [3], [5], [22].

2) A fully deterministic single-reflection model, which represents the model most commonly used in UHF RFID: the three-ray model, taking the line-of-sight path, the floor reflection, and the reflection at the opposite side of the gate into account, cf. [1], [18], [24][5]. The purely deterministic model thus considers the strongest specular reflections, but neglects weaker reflections and scattering.
3) A hybrid model incorporating both deterministic and stochastic components of the channel. The hybrid model

[5]Actually, the deterministic single-reflection model here is a "seven-ray" model, since it considers LOS, floor, backplanes, walls, and ceiling. However, the influence of walls and ceiling is negligible in comparison to portal and floor reflections, hence the model is basically equivalent to a three-ray model.

considers deterministic interreflections up to the 6-th order as well as scattered components and clusters via the same exponential APDP used by the purely stochastic model. Details regarding this model and its implementation can be found in [11, Chapter 3].

The central performance metric for passive UHF RFID systems is the ratio of tags that can be read while passing through the read zone. This ratio depends mostly on the incident power level at the tag (neglecting polarization mismatches and detuning) [25]–[27]. Consequently, channel models for UHF RFID focus almost solely on receive power levels, cf. [26]. The most common model is the three-ray model discussed above, represented by the single-reflection deterministic model here. Inside the gate this very simple model indeed nicely describes the incident power at some frequency in terms of shape and distribution, including the standing wave pattern, cf. Fig. 11. Outside the gate the mismatch is slightly more pronounced, cf. Fig. 11(b). This is also true for the stochastic as well as the more complex hybrid ("stoch.+det.") model. The offset between the measurement and the models is in the order of roughly $3-4$ dB and is likely caused by a distortion of the antenna gain patterns due to the close-by metal backplanes (projecting more energy to the outside of the portal).

Based on the result shown in Fig. 11 it seems safe to assume that a three-ray model of the RFID channel is suitable also for ranging and localization. This very common assumption, however, is wrong, as seen from Fig. 12, which shows CDFs of line-of-sight K-factor and RMS delay spread. Both values are off by factors. The mismatch is particularly drastic for the K-factor predicted by the purely stochastic model inside the gate (off by approx. 10 dB for the median) and for the K-factor predicted by the purely deterministic model outside the gate (off by 7 dB). Also the RMS delay spread inside and outside the gate predicted by the deterministic three-ray model is incorrect (off by a factor of five). Even the more complex hybrid model is not able to predict the channel parameters perfectly, although the mismatch is small in comparison.

Since K_{LOS} and τ_{RMS} are properties of the power-delay-profile, the mismatches should also be visible in the APDPs. A comparison between the APDPs for the metal portal derived from the measurements and APDPs predicted by the models is shown in Fig. 13. As can be seen, the simulated APDP for the purely stochastic channel model only fits the general shape of the APDP above path lengths of approximately 20 m. It thus neglects the very dominant deterministic reflections in the portal's backplanes as well as all clusters. The purely deterministic model, on the other hand, is able to reproduce the first two peaks of the APDP, but fails for path lengths above 7 m[6]. The reason for this failure are the missing scattered (stochastic) components as well as missing interreflections present at longer path lengths. Since all these components are considered by the hybrid model, its APDP follows the measured one quite well. An exception is the region inside the gate around path lengths of $10-20$ m, where a cluster is not modeled properly. This modeling problem is likely caused by the influence of the backplanes on the transmit antenna gain pattern, which is not covered by the simulation.

[6]The peaks for path lengths above 10 m are wall and ceiling reflections and would not be present for the three-ray model. Note that the wall reflections at 14 and 19 m become relevant outside the portal.

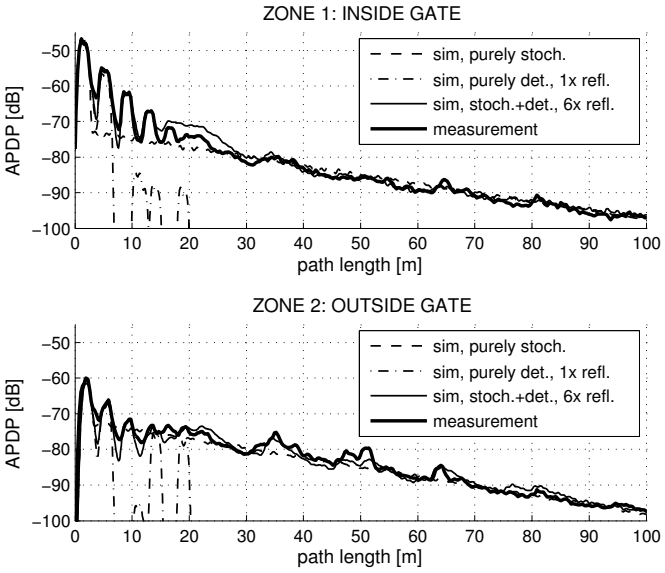

Fig. 13. Average power-delay-profiles (metal portal). Comparison between models of different complexity and measurement.

It should be mentioned that there is likely some room for improvement for all models, since no exhaustive optimization of the model parameters was done. However, a model that neglects important parts of the channel, such as the single-reflection deterministic or the purely stochastic model, cannot be optimized to fit all parameters at the same time. In particular, the low RMS delay spread for the single-reflection ("three-ray") model is an inherent problem created by the truncation of the CIR to reflections that are relatively close to the LOS (floor/gate-reflection), cf. Fig. 13. This truncation also leads to a limited worst-case range error and to easily resolvable MPCs in both angular and time domain, i.e., to overly optimistic errors for range finding as well as direction finding systems. Consequently, we strongly recommend the hybrid model for localization-related simulations of the UHF RFID channel.

VI. In-Depth Analyses: Gate with Pallet

Obviously, few products moved through warehouse portals are electromagnetically fully transparent, so the portal is not usually in its "empty" state. The following analyses assess the influence of a highly reflective/dispersive pallet on the channel's characteristics. To this end, the receiver antennas have been attached to the left side (closer to TX2) of a pallet filled with liquids and some metallized candy packages at heights of 0.5 through 1.3 m, cf. [20, Figs. 8–9]. The upper quarter of the receiver plane is visible to both transmitters, while the lower part has a clear line-of-sight only to TX2.

A. Discussion of Wideband Channel Parameters

Fig. 14 shows the spatial distribution of K_{LOS} and τ_{RMS} for the liquids pallet. The effects of the blocked LOS from TX1 are clearly visible in Fig. 14(a)(c), in particular at a

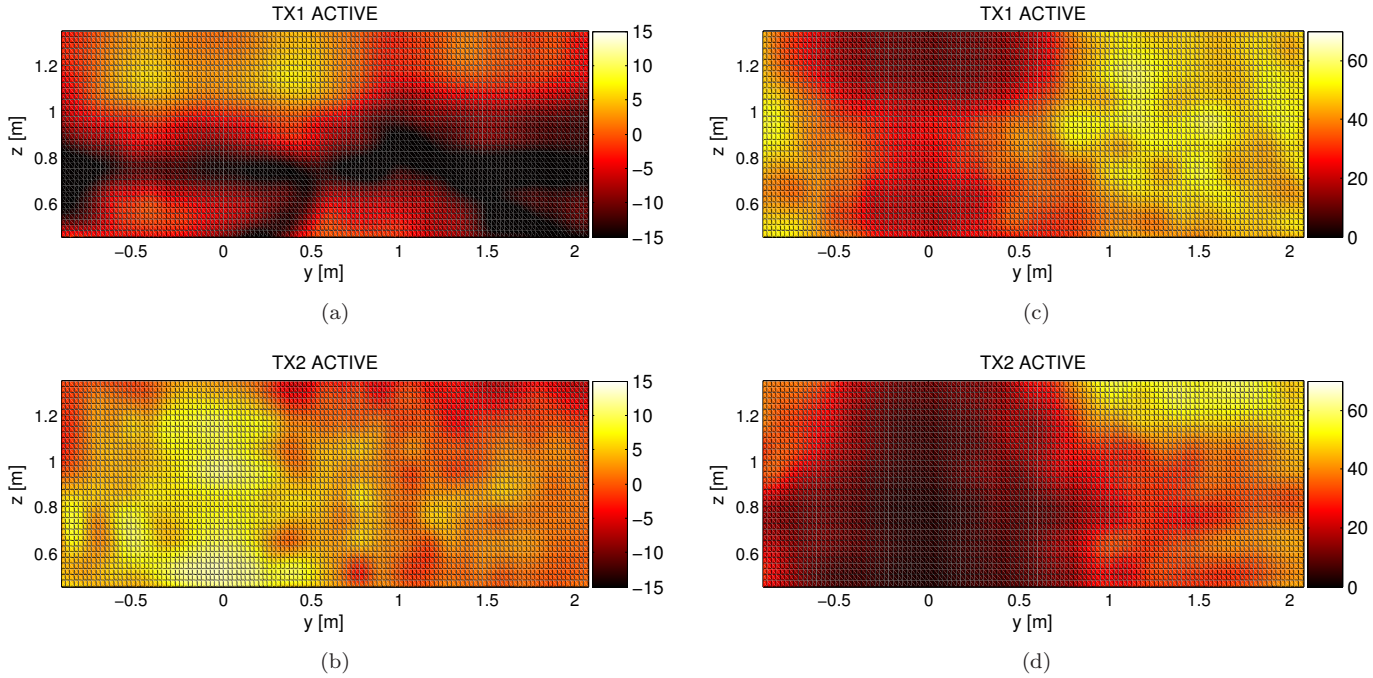

Fig. 14. Spatial distributions of (a)-(b) K-factor [dB] and (c)-(d) RMS delay spread [ns] at the left (TX2) side of the pallet while moving through the portal (cf. [20, Figs. 17, 18]). Liquids pallet, metal backplanes; view from TX1, portal center at y=0 m. The line-of-sight to TX1 is blocked for $z < 1.2$ m; TX2 always has a clear LOS.

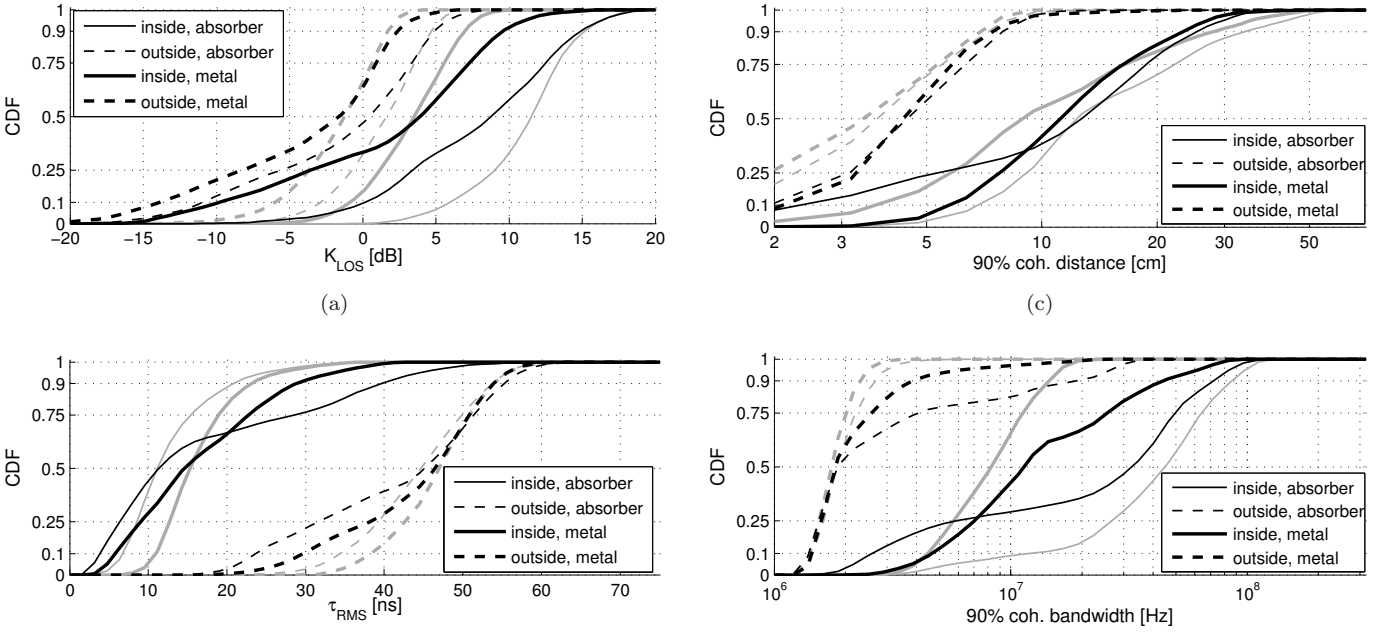

Fig. 15. CDFs for the liquids pallet: (a) K-factor, (b) RMS delay spread, (c) 90 % coherence distance, (d) 90 % coherence bandwidth. CDFs for the empty gate are displayed for comparison (gray curves). Note that the gate geometry limits the observable coherence distance to roughly 40 cm.

height of $z = 0.8$ m. The bottom of the pallet, on the other hand, consists of a wooden scaffold (EUR-EPAL pallet) that forms a narrow space between the liquids and the metal pallet mover, thus acting as a conduit for the signal sent by TX1. This causes a higher K-factor at $z = 0.6$ m and a decreased RMS delay spread, cf. Fig. 14(a)(c). Another effect of the pallet can be seen in the right part of Fig. 14(d): the pallet (at $z < 1.2$ m) keeps τ_{RMS} low by blocking several indirect MPCs when outside the gate ($y > 1$ m). This region also shows a constantly high K_{LOS} well above 0 dB despite the fact that it is outside TX2's mainlobe.

CDFs of K-factor, RMS delay spread, coherence distance, and coherence bandwidth for the liquids pallet scenario can be found in Fig. 15. Compared to the empty gate (which is shown

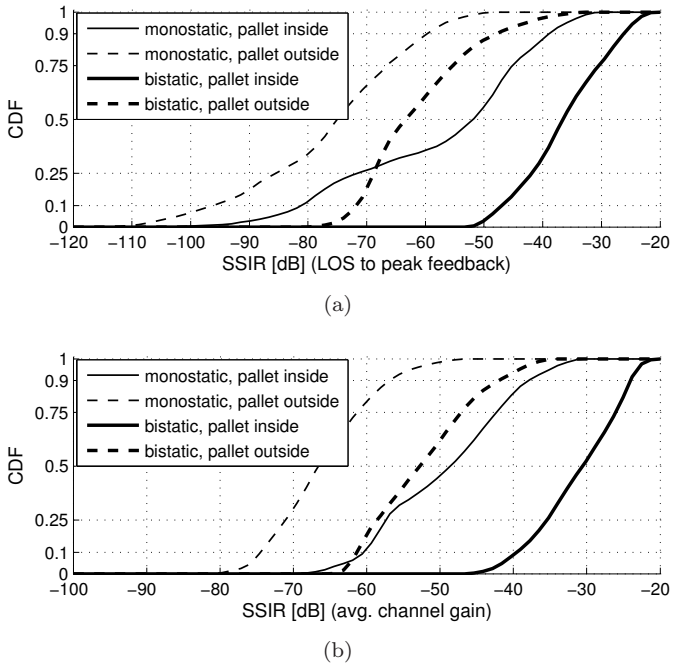

Fig. 16. CDFs of the measured signal-to-self-interference ratio SSIR [dB] for (a) ultra-wideband and (b) narrowband/wideband tag localization (liquids pallet, metal backplanes).

as a point of reference in these plots), almost all parameters span wider ranges, but with a clear tendency towards higher dispersiveness, i.e., reduced K_{LOS}, increased probability for high τ_{RMS}, etc. This is the case because the pallet blocks the line-of-sight from TX1, thus, for example, leading to K-factors as low as $-15\,\mathrm{dB}$ even inside the portal. However, in some cases the pallet blocks reflections instead of the LOS, thus increasing the K-factor and/or decreasing the RMS delay spread. An example here is the zone outside the portal, with lower RMS delay spreads, increased maximum coherence bandwidths, and slightly increased coherence distance compared to the empty portal.

B. Feedback Channels (Self-Interference)

Self-interference is a crucial problem for tag localization because it seriously limits the amplitude resolution left for the tag's backscatter signal and therefore also impairs the receiver sensitivity. For ultra-wideband systems, the relation between the backscatter LOS peak and the peak feedback component determines the best possible amplitude resolution for the backscatter LOS, while for narrowband systems the average power levels of backscatter and feedback are the determining factors.

Fig. 16(a) shows CDFs of the signal-to-self-interference ratio (SSIR) for the metal portal, calculated between the backscatter LOS component and the peak feedback component (SSIR for UWB systems). The SSIR ranges from -100 through $-25\,\mathrm{dB}$ for the measurements, where the lowest values are caused by a blocked LOS component. Note that the interference increases dramatically when the pallet (with the tag attached) is outside the portal, since this maximizes the gate reflections (not blocked by the pallet) while at the same time minimizing the backscatter LOS component (tag outside transmitter mainlobe). Moreover, the SSIR is at least $10\,\mathrm{dB}$ lower for the monostatic setup compared to the bistatic antenna configuration. The average self-interference observed by narrowband and wideband systems is slightly lower in comparison since the average power is less sensitive to a blocked LOS component. See Fig. 16(b) for the corresponding CDF plots.

A typical goal of tag localization in UHF RFID is the identification of stray reads outside the intended read zone. In these cases, the SSIR is expected to be extremely low, as the tag is outside the antenna main lobe while clutter is within. This makes feedback mitigation one of the primary challenges in passive UHF RFID tag localization.

VII. Reader - Tag - Reader: Backscatter Channel

Most results presented in this paper are based on individual channels between reader and tag. This keeps the analyses independent of the used setup (monostatic/bistatic) as well as comparable to other results in the literature [3]–[5] and applicable to non-backscatter systems, e.g. [6], [7]. However, current passive UHF RFID systems use backscatter signaling, hence the localization performance is determined by the overall backscatter channel instead of the individual constituent channels. Backscatter channels are degenerate channels, with more pronounced fading [28]–[30] and with lower K_{LOS} and higher τ_{RMS} [8] than for the individual up- and downlink channels. Moreover, correlation between the constituent channels, such as in monostatic setups, additionally decreases K_{LOS} and increases τ_{RMS} [8]. K_{LOS} and τ_{RMS} of the backscatter channel can be calculated from K_{LOS} and τ_{RMS} of the constituent channels using the following formulas.

The backscatter K-factor can be approximated independent of the shapes of the single-channel PDPs via [8]

$$K_{\mathrm{LOS,bs}} = \left(1 - \frac{\alpha_{\mathrm{K}}}{2}\right) \cdot \frac{K_{\mathrm{LOS},1} \cdot K_{\mathrm{LOS},2}}{1 + K_{\mathrm{LOS},1} + K_{\mathrm{LOS},2}}, \qquad (1)$$

where $K_{\mathrm{LOS},1}$ and $K_{\mathrm{LOS},2}$ are the K-factors of the two constituent channels and $0 \leq \alpha_{\mathrm{K}} \leq 1$ represents correlation between both channels. The RMS delay spread of the backscatter channel based on the constituent channel parameters is approximated via [8]

$$\tau_{\mathrm{RMS,bs}} = \sqrt{\tau_{\mathrm{RMS},1}^2 + \tau_{\mathrm{RMS},2}^2 + 2 \cdot \alpha_\tau \cdot \tau_{\mathrm{RMS},1} \cdot \tau_{\mathrm{RMS},2}}, \qquad (2)$$

where $0 \leq \alpha_\tau \leq 1$ again represents correlation. Unlike for the K-factor, α_τ depends on the shapes of the constituent PDPs for correlated channels and only approaches $\alpha_\tau = 1$ for high K-factors [8]. For fully correlated up- and downlink channels in monostatic setups, this parameter can be approximated by

$$\alpha_{\tau,\mathrm{monostat.}} \approx \frac{K_{\mathrm{LOS},1}}{10 + K_{\mathrm{LOS},1}}, \qquad (3)$$

with $K_{\mathrm{LOS},1} = K_{\mathrm{LOS},2}$ due to the full correlation [8]. Although strictly speaking (3) is only valid for exponential PDPs, the formula works well also for non-exponential PDPs, cf. [31].

Fig. 17 shows CDFs of K-factor and RMS delay spread calculated from the single-channel values via the above equations. Note that the backscatter K-factor rarely exceeds $0\,\mathrm{dB}$

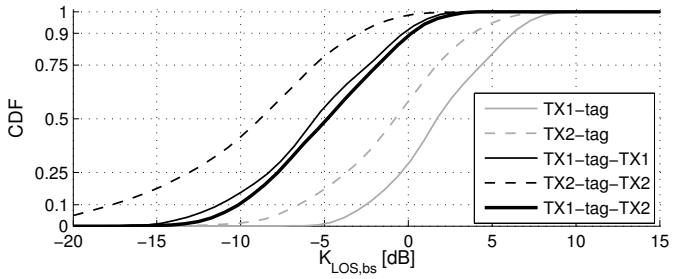

(a)

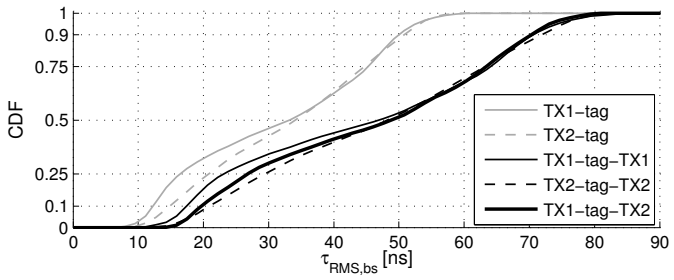

(b)

Fig. 17. CDFs of backscatter (a) K-factor and (b) RMS delay spread according to (1)–(3) for mono- and bistatic reader setups (empty portal, metal backplanes). Single-channel CDFs are displayed for comparison (gray curves).

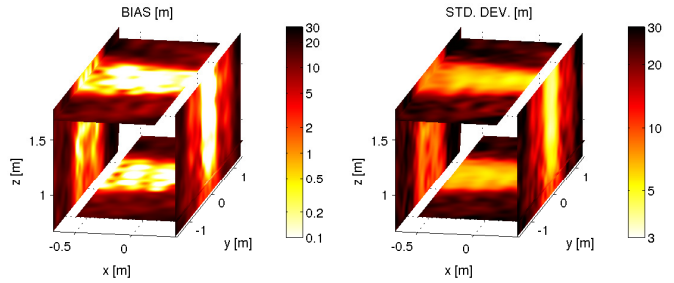

Fig. 18. Bias and standard deviation for a narrowband ranging approach [12] with 1 MHz bandwidth (empty portal, metal backplanes, TX1).

even for the empty portal (best case). Consequently, the LOS component cannot be assumed to be dominant in UHF RFID tag localization. Also the RMS delay spread is considerable, in particular when taking into account that the minimum values around 15 ns ($\sim$4.5 m) are reached at distances well below 1 m and in direct line-of-sight.

VIII. Expected Performance of Ranging Methods

This section provides a brief discussion of the achievable ranging performance in UHF RFID portals in the light of the channel analyses presented in this paper. The figures in this section have been created via simulation using the measured channel impulse responses. Please refer to [11] for further details and analyses.

A. Narrowband Ranging

Until today, most ranging systems in UHF RFID focus on narrowband signals [1]. However, given the fact that narrowband ranging requires a dominant LOS and in the light of the K-factors and RMS delay spreads presented in this paper, it is safe to assume that any narrowband range estimate will show a considerable bias and high variance. This is indeed the case, as can be seen in Fig. 18, which depicts bias and standard deviation for a narrowband ranging approach [12] with 1 MHz bandwidth. The estimates show a bias of up to 3 m and and a standard deviation of $3-15$ m even inside the portal, with a considerable increase for the region outside the portal.

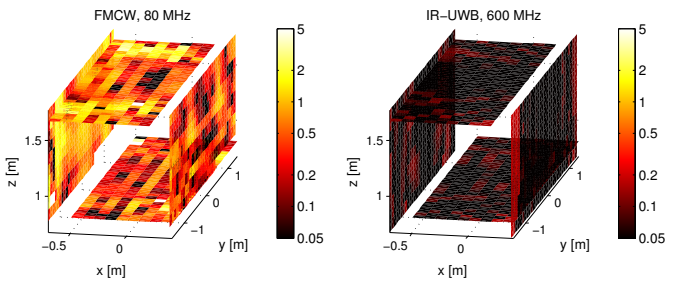

Fig. 19. Range error for wideband and ultra-wideband ranging methods (empty portal, metal backplanes, TX1). The spatial resolutions of these systems are 1.9 m (FMCW) and 0.5 m (UWB) respectively.

B. Wideband and Ultra-Wideband Ranging

Only recently advances were made into more wideband ranging methods in UHF RFID, e.g., [32]–[34], including a proof of concept for UWB-based ranging based on measurements in an environment largely comparable to a portal [35].

Fig. 19 shows the (instantaneous) range error for 80 MHz frequency-modulation continuous-wave (FMCW) radar and the range error of a 600 MHz impulse-radio (IR) UWB method. Note that the spatial resolution of $c/2B$, where c is the speed of light and B is the bandwidth of the system, is reached and even exceeded in this environment, cf. [19]. Further analyses can be found in [11] and [19].

Notably, the strong specular reflections in the portal backplanes could be used to further increase the localization accuracy for UWB localization by using them as virtual transmitters [36]. Two prerequisites of this method, namely the presence of strong reflectors and a fixed and known geometry, are met for UHF portals.

IX. Conclusion

A comprehensive investigation w.r.t. ranging and localization was presented of the UHF RFID channel, based on measurements inside a warehouse portal. The influence of reflecting/absorbing backplanes as well as the effects of a reflective pallet on the channel was discussed in detail, including the feedback in mono- and bistatic setups. Furthermore, the channel was analyzed for deterministic components and compared to a number of channel models.

It was shown that the UHF RFID backscatter channel has surprisingly low K-factors and high RMS delay spreads given the short range and the directive antennas. K-factors w.r.t. the LOS component are typically in the range of 0 dB and below for metal-shielded portals and RMS delay spreads are above 15 ns even in direct line-of-sight at ranges well below 1 m. As

a consequence, the direct path is rarely the dominant path in this typical UHF RFID setup.

It was also shown that neither fully stochastic nor fully deterministic channel models are suitable for the UHF RFID channel. The classical three-path model in particular produces far too optimistic multipath propagation parameters and thus causes overly accurate localization results in simulations. A slightly more complex hybrid channel model combining deterministic (specular) with stochastic (scattered) multipath components is able to correctly predict the channel parameters, including the channel impulse response.

X. Acknowledgments

We would like to express our gratitude to Grzegorz Adamiuk (Karlsruhe Institute of Technology) for designing the antennas used in the measurements, Giuliano Manzi, Martin Rampetsreiter, Gerald Wiednig, and Alexey Nazarov (NXP) for their invaluable help with the measurement setups, as well as Albert Angstenberger (Taconic) for providing the substrates used for the antennas. We would also like to thank NXP for providing the environment for all measurements.

References

[1] P. V. Nikitin, R. Martinez, S. Ramamurthy, H. Leland, G. Spiess, and K. V. S. Rao, "Phase based spatial identification of UHF RFID tags," in *Proc. IEEE Int RFID Conf*, 2010, pp. 102–109.

[2] Z. Sahinoglu, S. Gezici, and I. Guvenc, *Ultra-wideband Positioning Systems: Theoretical Limits, Ranging Algorithms, and Protocols*. Cambridge University Press, 2008, ISBN-13: 978-0521873093.

[3] L. J. Greenstein, S. S. Ghassemzadeh, S.-C. Hong, and V. Tarokh, "Comparison study of UWB indoor channel models," *IEEE Trans. Wireless Commun.*, vol. 6, no. 1, pp. 128–135, 2007.

[4] M. S. Varela and M. G. Sánchez, "RMS delay and coherence bandwidth measurements in indoor radio channels in the UHF band," *IEEE Trans. Veh. Technol.*, vol. 50, no. 2, pp. 515–525, Mar. 2001.

[5] A. F. Molisch, D. Cassioli, C.-C. Chong, S. Emami, A. Fort, B. Kannan, J. Karedal, J. Kunisch, H. G. Schantz, K. Siwiak, and M. Z. Win, "A comprehensive standardized model for ultrawideband propagation channels," *IEEE Trans. Antennas Propag.*, vol. 54, no. 11, pp. 3151–3166, 2006.

[6] Z. Zou, T. Deng, Q. Zou, M. D. Sarmiento, F. Jonsson, and L.-R. Zheng, "Energy detection receiver with TOA estimation enabling positioning in passive UWB-RFID system," in *Proc. IEEE Int Ultra-Wideband (ICUWB) Conf*, vol. 2, 2010, pp. 1–4.

[7] M. B. Nejad, "Ultra wideband impulse radio for wireless sensing and identifiation," PhD thesis, Royal Institute of Techn., Sweden, 2008.

[8] D. Arnitz, U. Muehlmann, and K. Witrisal, "Wideband characterization of backscatter channels: Derivations and theoretical background," accepted for publication (IEEE Trans. Antennas Propag.). [Online]. Available: http://www.spsc.tugraz.at/publications

[9] A. Molisch, *Wireless Communications*, 1st ed. John Wiley & Sons, 2005, ISBN-13: 978-0470848876.

[10] T. S. Rappaport, *Wireless Communications*, 2nd ed. Prentice Hall International, 2002, ISBN-13: 978-0130422323.

[11] D. Arnitz, "Tag localization in passive UHF RFID," PhD thesis, Graz Univ. of Techn., Austria, 2011. [Online]. Available: http://www.spsc.tugraz.at/publications

[12] D. Arnitz, U. Muehlmann, and K. Witrisal, "Multi-frequency continuous-wave radar approach to ranging in passive UHF RFID," *IEEE Trans. Microw. Theory Tech.*, vol. 57, no. 5, pp. 1398–1405, Jul. 2009. [Online]. Available: http://www.spsc.tugraz.at/publications

[13] K. Witrisal, Y.-H. Kim, and R. Prasad, "A new method to measure parameters of frequency-selective radio channels using power measurements," *IEEE Trans. Commun.*, vol. 49, no. 10, pp. 1788–1800, Oct. 2001, 10.1109/26.957401.

[14] A. Paulraj, R. Nabar, and D. Gore, *Introduction to Space-Time Wireless Communications*, 1st ed. Cambridge University Press, 2003, ISBN-13: 9-780521826150.

[15] B. Yanakiev, P. Eggers, G. F. Pedersen, and T. Larsen, "Assessment of the physical interface of UHF passive tags for localization," in *Proc. 1st Int EURASIP RFID Workshop*, 2007, pp. 1–4.

[16] X. Li, Y. Zhang, and M. G. Amin, "Multifrequency-based range estimation of RFID tags," in *Proc. IEEE Int RFID Conf*, 2009, pp. 147–154.

[17] Y. Zhang, X. Li, and M. G. Amin, "Array processing for RFID tag localization exploiting multi-frequency signals," in *SPIE Symposium on Defense, Security, and Sensing*, 2009.

[18] U. Muehlmann, G. Manzi, G. Wiednig, and M. Buchmann, "Modeling and performance characterization of UHF RFID portal applications," *IEEE Trans. Microw. Theory Tech.*, vol. 57, no. 7, pp. 1700–1706, 2009.

[19] G. Li, D. Arnitz, R. Ebelt, U. Muehlmann, K. Witrisal, and M. Vossiek, "Bandwidth dependence of CW ranging to UHF RFID tags in severe multipath environments," in *Proc. IEEE Int RFID Conf*, Orlando, Florida, Apr. 2011, pp. 19–25. [Online]. Available: http://www.spsc.tugraz.at/publications

[20] D. Arnitz, G. Adamiuk, U. Muehlmann, and K. Witrisal, "UWB channel sounding for ranging and positioning in passive UHF RFID," in *11th COST2100 MCM*, Aalborg, Denmark, Jun. 2010. [Online]. Available: http://www.spsc.tugraz.at/publications

[21] The PARIS Simulation Framework. Graz University of Technology, NXP Semiconductors. Open-Source (GNU GPL v3). [Online]. Available: http://www.spsc.tugraz.at/tools/paris-osf

[22] J. Karedal, S. Wyne, P. Almers, F. Tufvesson, and A. F. Molisch, "A measurement-based statistical model for industrial ultra-wideband channels," *IEEE Trans. Wireless Commun.*, vol. 6, no. 8, pp. 3028–3037, 2007.

[23] C. L. Holloway, M. G. Cotton, and P. McKenna, "A model for predicting the power delay profile characteristics inside a room," *IEEE Trans. Veh. Technol.*, vol. 48, no. 4, pp. 1110–1120, 1999.

[24] Y. Han and H. Min, "System modeling and simulation of RFID," in *Auto-ID Labs Whitepaper*, 2005. [Online]. Available: http://www.autoidlabs.org/uploads/media/AUTOIDLABS-WP-HARDWARE-010.pdf

[25] D. M. Dobkin, *The RF in RFID*. Elsevier, 2007, ISBN-13: 978-0750682091.

[26] G. Marrocco, E. Di Giampaolo, and R. Aliberti, "Estimation of UHF RFID reading regions in real environments," *IEEE Antennas Propag. Mag.*, vol. 51, no. 6, pp. 44–57, 2009.

[27] S. R. Aroor and D. D. Deavours, "Evaluation of the state of passive UHF RFID: An experimental approach," *IEEE Systems Journal*, vol. 1, no. 2, pp. 168–176, 2007.

[28] J. D. Griffin and G. D. Durgin, "Complete link budgets for backscatter-radio and RFID systems," *IEEE Antennas Propag. Mag.*, vol. 51, no. 2, pp. 11–25, 2009.

[29] ——, "Link envelope correlation in the backscatter channel," *IEEE Commun. Lett.*, vol. 11, no. 9, pp. 735–737, 2007.

[30] D. Kim, M. A. Ingram, and W. W. Smith, "Measurements of small-scale fading and path loss for long range RF tags," *IEEE Trans. Antennas Propag.*, vol. 51, no. 8, pp. 1740–1749, Aug. 2003.

[31] D. Arnitz, U. Muehlmann, and K. Witrisal, "Wideband characterization of backscatter channels," in *Proc. Europ. Wireless Conf*, Vienna, Austria, Apr. 2011, pp. 205–211. [Online]. Available: http://www.spsc.tugraz.at/publications

[32] F. Guidi, A. Sibille, D. Dardari, and C. Roblin, "UWB RFID backscattered energy in the presence of nearby metallic reflectors," in *Proc. 5th European Conf. Antennas and Propagation (EUCAP)*, 2011, pp. 1425–1429.

[33] D. Dardari, R. D'Errico, C. Roblin, A. Sibille, and M. Z. Win, "Ultra-wide bandwidth RFID: The next generation?" *Proc. IEEE*, vol. 98, no. 9, pp. 1570–1582, 2010.

[34] J. Heidrich, D. Brenk, J. Essel, S. Schwarzer, K. Seemann, G. Fischer, and R. Weigel, "The roots, rules, and rise of RFID," *IEEE Microw. Mag.*, vol. 11, no. 3, pp. 78–86, 2010.

[35] D. Arnitz, U. Muehlmann, and K. Witrisal, "UWB ranging in passive UHF RFID: Proof of concept," *IET Electron. Letters*, vol. 46, no. 20, pp. 1401–1402, Sep. 2010. [Online]. Available: http://www.spsc.tugraz.at/publications

[36] P. Meissner, C. Steiner, and K. Witrisal, "UWB positioning with virtual anchors and floor plan information," in *Proc. 7th Workshop Positioning Navigation and Communication (WPNC)*, 2010, pp. 150–156. [Online]. Available: http://www.spsc.tugraz.at/publications

Daniel Arnitz Daniel Arnitz received the Master degree Dipl.-Ing.(FH) in electrical engineering from the University of Applied Sciences FH Joanneum Kapfenberg, Austria, in 2005, and a Ph.D. degree (Dr. techn.) from Graz University of Technology, Austria, in 2011 (both degrees with honors). His Ph.D. thesis covers the field of tag localization in passive UHF RFID and his diploma thesis focused on a feasibility study of (burst) error correcting codes for long-range RFID systems. He is currently with the Signal Processing and Speech Communication Laboratory of Graz University of Technology, Austria. His research interests include RF positioning and radar systems, channel and system modeling, ultra-wideband technologies, and nonlinear systems.

Klaus Witrisal received the Dipl.-Ing.degree in electrical engineering from Graz University of Technology, Austria, in 1997, the Ph.D. degree (cum laude) from Delft University of Technology, The Netherlands, in 2002, and the Venia Docendi (Habilitation) from Graz University of Technology in 2009. From 1997 to 2001, he was a Ph.D. student and research engineer at Delft University of Technology. Currently, he is an associate professor at the Signal Processing and Speech Communication Laboratory (SPSC) of Graz University of Technology. His research interests are in signal processing for broadband and UWB wireless communications, propagation channel modeling, and positioning. He is co-chair of the MTT/COM Society of the IEEE Austria Section.

Ulrich Muehlmann (M'05) has received his master degree (Dipl.-Ing. in telematics) at Graz University of Technology in 2000. In 2001 he started research work in Optical Tracking at the Department of Electrical Measurement and Measurement Signal Processing (TU Graz, Austria). In November 2005 he received his Ph.D.-degree (Dr. at Graz Univ. of Techn.) with honours. Since 2005 he is with NXP Semiconductors (former Philips Semiconductors) working in the field of UHF RFID technology focused on systems and analog innovation. He is author and/or co-author of several publications in the field of Optical Tracking, Machine Vision and RFID.